Realizing enhanced cyclability of cactus-like $NiCo_2O_4$ nanocrystals anode enabled by molecular layer deposition

*Jia-Bin Fang, Qiang Ren, Chang Liu, Ji-An Chen, Di Wu, Ai-Dong Li**

National Laboratory of Solid State Microstructures, Department of Materials Science and Engineering, College of Engineering and Applied Sciences, Jiangsu Key Laboratory of Artificial Functional Materials, Collaborative Innovation Center of Advanced Microstructures, Nanjing University, Nanjing 210093, People's Republic of China

Electronic mail: adli@nju.edu.cn

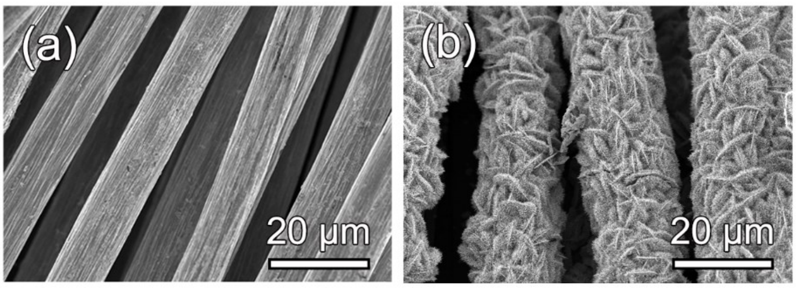

Figure S1. SEM images of bare CC (a) and cactus-like $NiCo_2O_4$ flakes on CC (b).

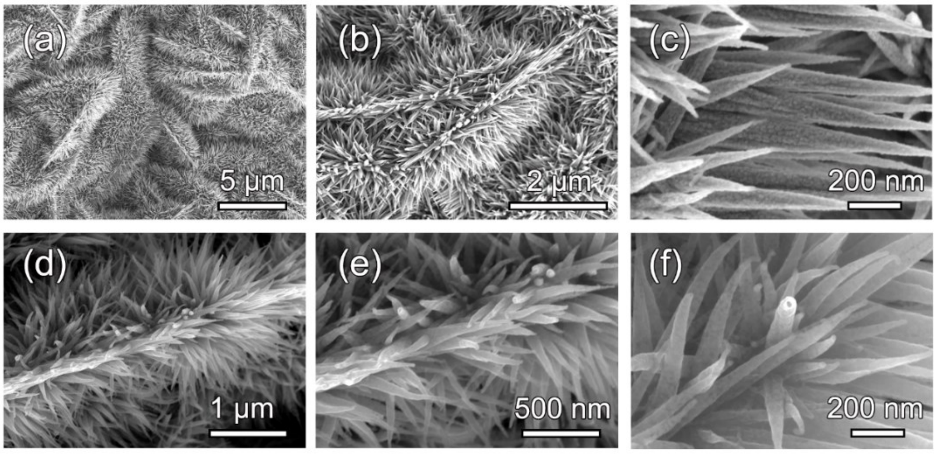

Figure S2. SEM images of (a-c) bare $NiCo_2O_4$ and (d-f) $NiCo_2O_4$@Al_2O_3/carbon with different magnifications.

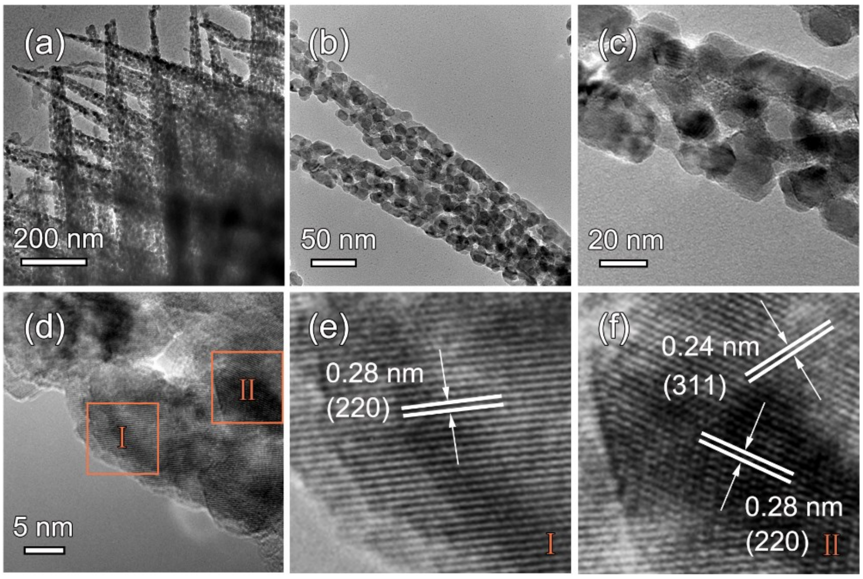

Figure S3. (a, b) Low-magnification TEM images, (c-f) high-magnification TEM images of bare $NiCo_2O_4$.

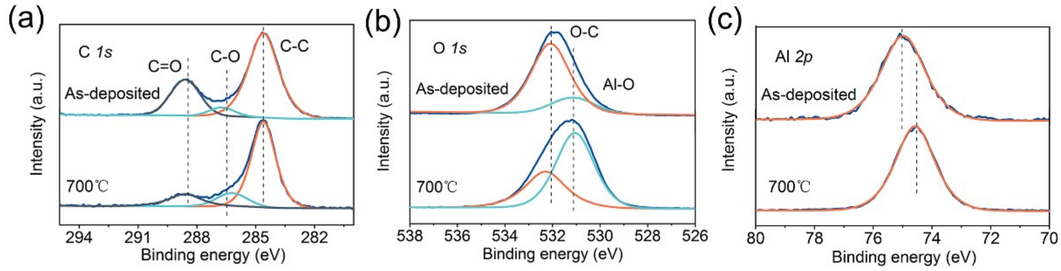

Figure S4. XPS spectra of as-deposited and annealed alucone films on Si: (a) C 1s, (b) O 1s and (c) Al 2p.

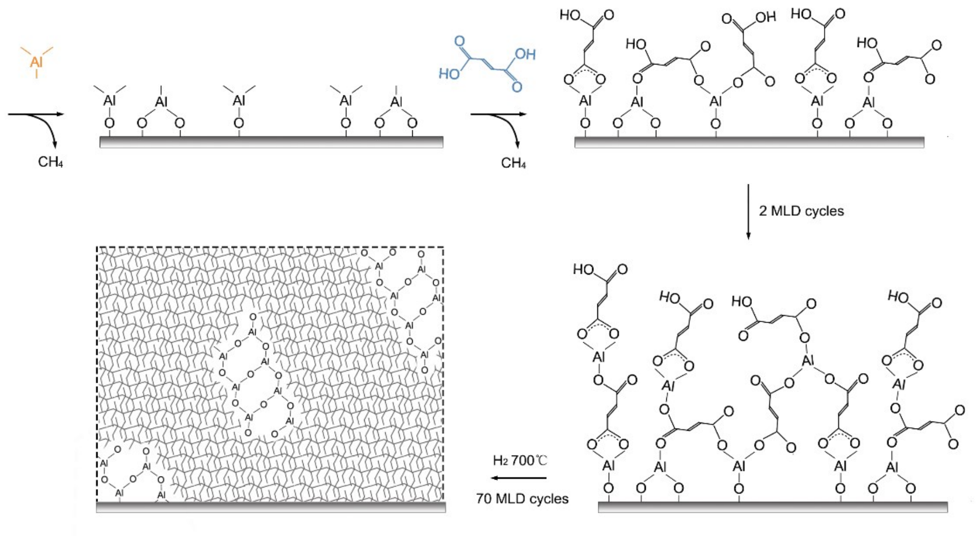

Figure S5. A schematic of the possible reaction mechanism and subsequent pyrolysis for the TMA-fumaric acid film.

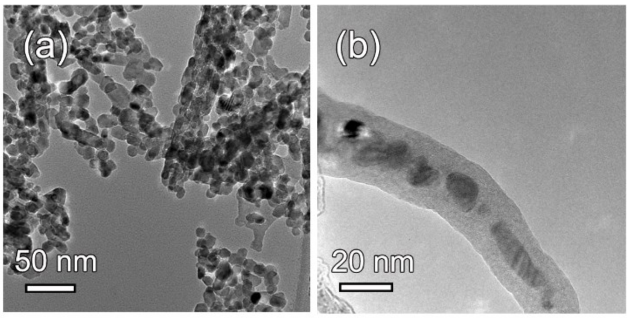

Figure S6. TEM images of (a) bare $NiCo_2O_4$ and (b) $NiCo_2O_4$@Al_2O_3/carbon ultrasonic dispersion for 10 min in alcohol.

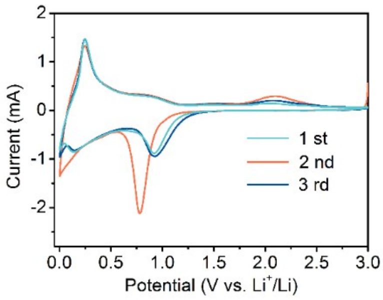

Figure S7. CV curves of bare $NiCo_2O_4$ for the first three cycles at the scan rate of 0.1 mV s^{-1}.

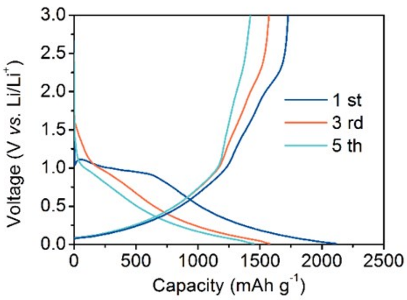

Figure S8. Charge/discharge curves for the 1st, 3rd and 5th cycles at 200 mA g^{-1} of bare $NiCo_2O_4$ electrode.

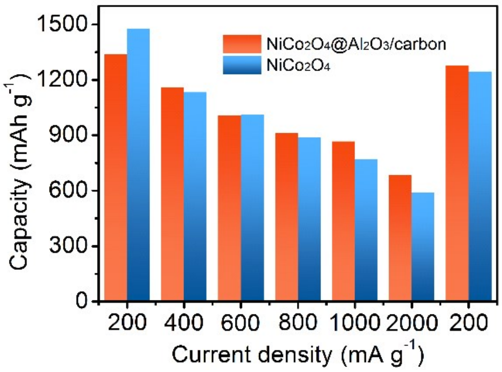

Figure S9. Column view of rate performance of $NiCo_2O_4@Al_2O_3$/carbon and bare $NiCo_2O_4$ electrodes.

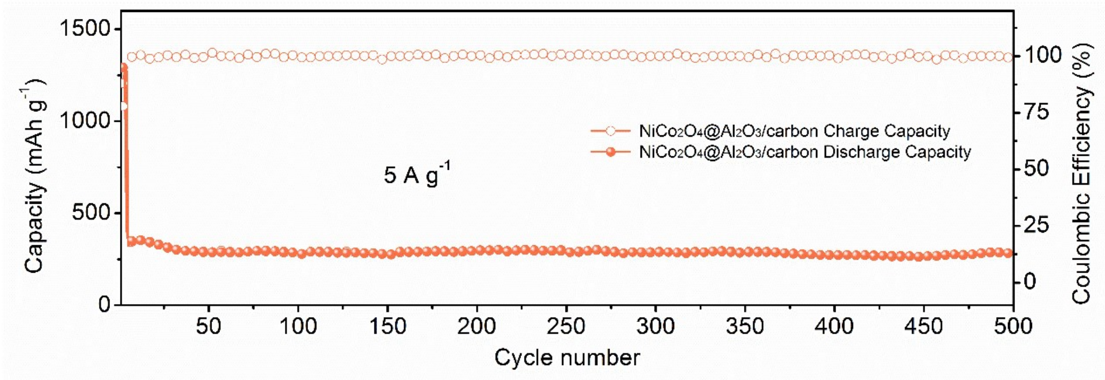

Figure S10. Cycling performance of $NiCo_2O_4@Al_2O_3$/carbon electrode at 5 A g^{-1}.

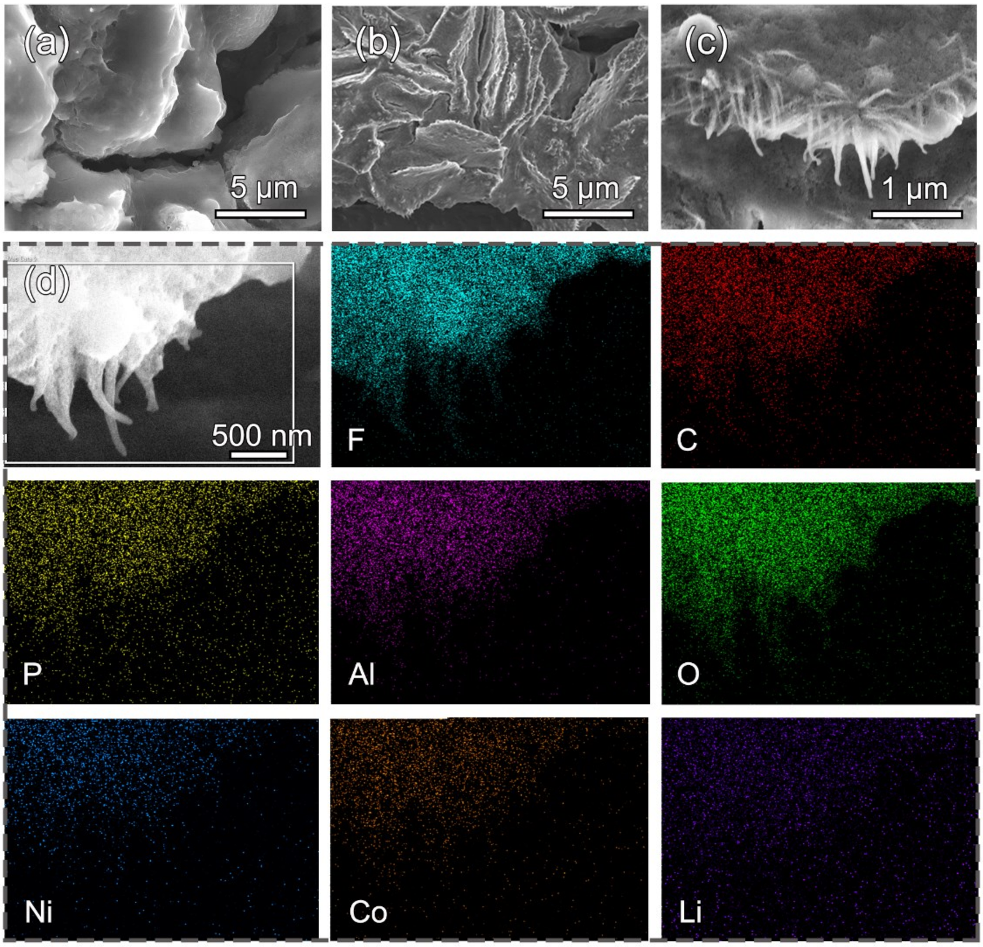

Figure S11. (a) SEM image for cycled $NiCo_2O_4$ anode after 200 cycles; (b, c) SEM images and (d) corresponding EDS mapping of elemental F, C, P, Al, O, Ni, Co, and Li for the cycled $NiCo_2O_4$@Al_2O_3/carbon anode after 200 cycles.

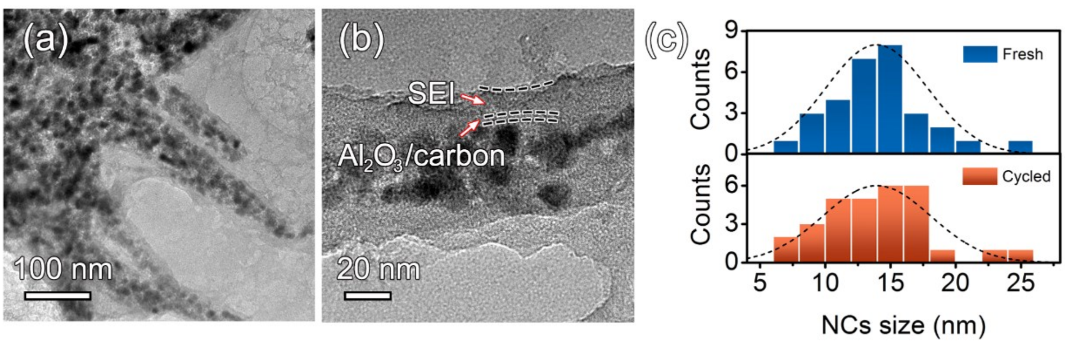

Figure S12. (a, b) TEM images of $NiCo_2O_4$@Al_2O_3/carbon electrode after 200 charge/discharge cycles at 2 A g^{-1}. The thickness of SEI layer is ~10 nm indicated by the upper arrow; (c) Distribution of $NiCo_2O_4$ NCs size in $NiCo_2O_4$@Al_2O_3/carbon before and after cycling.

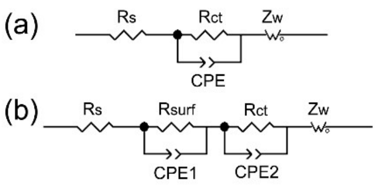

Figure S13. Equivalent electrical circuit diagram.

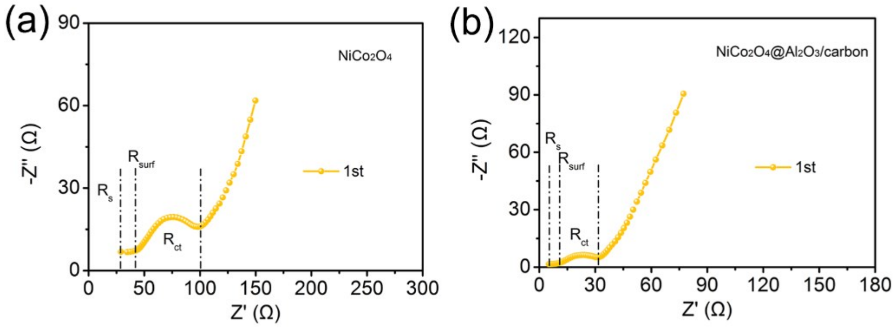

Figure S14. Electrochemical impedance spectra of (a) bare $NiCo_2O_4$ and (b) $NiCo_2O_4$@Al_2O_3/carbon after the first cycle.

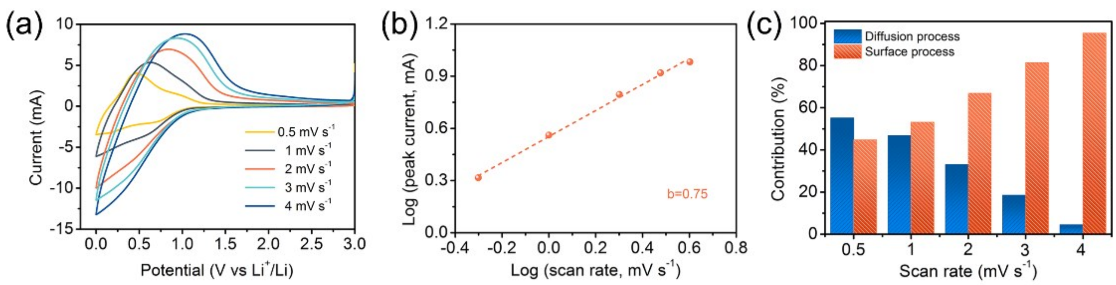

Figure S15. Kinetics analyses of electrochemical behavior: (a) CV profiles of $NiCo_2O_4$@Al_2O_3/carbon anode at various scan rates; (b) Relationship between the log (peak current) and log (scan rate); (c) Contribution ratios of capacitive and diffusion-controlled charge storage at different scan rates.

Table S1

Comparison of Li-ion storage performances between recent reported $NiCo_2O_4$ based anodes and this work.

Anode material	Current density (A g^{-1})	Cycle number	Reversible capacity (mAh g^{-1})	Refs.
$NiCo_2O_4$@N-doped carbon submicrospheres	1	1000	371.4	[1]
$NiCo_2O_4$@ZIF-67/GO	0.5	80	1025	[2]
	2	80	740	
$NiCo_2O_4$@Ni-B composites	0.5	500	865	[3]
$NiCo_2O_4$-holey graphene	0.178	450	931.2	[4]
Fe_2O_3/$NiCo_2O_4$ composite	0.178	200	1528	[5]
$NiCo_2O_4$@MnO_2 composites	1	100	841.9	[6]
Ni-$NiCo_2O_4$@$ZnCo_2O_4$	0.1	70	1571.9	[7]
	1	600	1097.5	
$NiCo_2O_4$/CNT	1	200	1673	[8]
$NiCo_2O_4$@TiO_2	2	800	749.74	[9]
PPC/$NiCo_2O_4$	2	1100	363	[10]
$NiCo_2O_4$@Al_2O_3/carbon	0.2	150	1574	**This work**
	2	200	931.2	
	5	500	280	

References

1. D. K. Denis, Z. Wang, X. Sun, F. U. Zaman, J. Zhang, L. Hou, J. Li and C. Yuan, *ACS applied materials & interfaces*, 2019, **11**, 32052-32061.
2. Y. Kuang, C. Chen, K. Li, B. Hao, J. Ma, Y. Liao, H. Mao and F. Huo, *Nanoscale*, 2019, **11**, 15166-15172.
3. M. Li, Q. Zhou, C. Ren, N. Shen, Q. Chen, J. Zhao, C. Guo, L. Zhang and J. Li, *Nanoscale*, 2019, **11**, 22550-22558.
4. D. Yuan, Y. Dou, L. Xu, L. Yu, N. Cheng, Q. Xia, L. Hencz, J. Ma, S. X. Dou and S. Zhang, *Journal of Materials Chemistry A*, 2020, **8**, 13443-13451.
5. J. Liu, Y. Ding, T. Han, J. Long, X. Pei, Y. Luo, W. Bao, X. Lin and H. Zhang, *Chemical communications*, 2020, **56**, 2618-2621.
6. Z. Zhang, Y. Huang, J. Yan, C. Li, X. Chen and Y. Zhu, *Applied Surface Science*, 2019, **473**, 266-274.
7. H. Xin, D. Li, L. Shi, M. Ji, Y. Lin, J. Yu, B. Yang, C. Li and C. Zhu, *Chemical Engineering*

Journal, 2018, **341**, 601-609.

8. S.-K. Park, S. H. Yang and Y. C. Kang, *Chemical Engineering Journal*, 2018, **349**, 214-222.
9. P. Liu, Q. Ru, Z. Wang, B. Wang, Q. Guo, P. Zhang, X. Hou, S. Su and F. C.-C. Ling, *Chemical Engineering Journal*, 2018, **350**, 902-910.
10. C. Zhang, Z. Xie, W. Yang, Y. Liang, D. Meng, X. He, P. Liang and Z. Zhang, *Journal Of Power Sources*, 2020, **451**.